Hindawi
Mathematical Problems in Engineering
Volume 2021, Article ID 9285832, 9 pages
https://doi.org/10.1155/2021/9285832

Research Article

Study on the Formation Mechanism of Rock Burst Caused by Seam Floor Slip under an Ultrathick Conglomerate

Zhiyong Ma,[1,2,3] **Wenkai Feng**,[1] **Zhen Wang**,[2,3] **Fujin Lin**,[2,3] **and Dayong Li**[2,3]

[1]*State Key Laboratory of Geohazard Prevention and Geoenvironment Protection, Chengdu University of Technology, Chengdu 610059, China*
[2]*State Key Laboratory of the Gas Disaster Detecting, Preventing and Emergency Controlling, Chongqing 400037, China*
[3]*CCTEG Chongqing Research Institute, Chongqing 400037, China*

Correspondence should be addressed to Zhiyong Ma; mazhiyong@stu.cdut.edu.cn and Wenkai Feng; fengwenkai@cdut.cn

Received 15 October 2021; Revised 9 November 2021; Accepted 11 November 2021; Published 17 December 2021

Academic Editor: Gan Feng

A rock burst accident occurred on coalface 13230 of the Gengcun Coal Mine in Henan Province. Through a field investigation, theoretical analysis, and microseismic monitoring, we studied how the rock burst, which was caused by overall seam floor slip and instability, occurring under an ultrathick conglomerate. Because the overlying ultrathick conglomerate in the mined-out zone close to coalface 13230 had been inadequately mined, the leading section of the coalface was under a high level of stress. Combined with the tectonic stresses from the F_{16} faultage and the soft floor structure, these factors caused the floor of this coalface to trigger the overall slip-type rock burst. In this paper, an estimation model of the ultimate bearing capacity of a seam floor under an ultrathick conglomerate and the advancing abutment pressure on the coalface is presented. This model is used to show that the ultimate bearing capacity of the seam floor on coalface 13230 is 26.3 MPa, and the abutment pressure is far more than the floor bearing capacity. We also present pressure relief and reinforced supporting measures, which can effectively prevent floor slip-type rock bursts from occurring. The results of this study provide a reference for the prevention and control of floor slip-type rock bursts in coal mining under an ultrathick conglomerate.

1. Introduction

A rock burst is the sudden release of elastic energy accumulated by a coal and rock mass. Such events have become a common type of dynamic disaster that seriously threatens mine production safety [1–8]. The average thickness of the coal seam in the Yima Coal Field in Henan is 10 m. The roof of this seam is made of an ultrathick conglomerate. The top coal mining approach used in this area leaves clear traces of rock bursts. Unlike common dynamic rock burst disasters, rock bursts in the Yima Coal Field occur on the seam floor. As the burial depth and mining intensity increase, more and more macroenergy events have occurred on the stope of the Yima Coal Field in recent years. These events have decreased the area of the two roadways on the coalface and resulted in casualties and damages to facilities, posing a major threat to production safety.

Rock bursts may be caused by many factors. Based on statistics of rock burst accidents, Zhang et al. [2] and Guo et al. [9] found that these factors can include coal seam overburden, geological conditions, burst tendency, and excavation activities. Jiang [10] et al. studied the evolution characteristics of the rock burst risk at different mining widths in deep mines. Based on the coupling hypothesis of static and dynamic stresses, Wu et al. [11] studied the formation mechanism of rock bursts. Wang et al. [12] and Zhang et al. [13] studied the mechanism of rock bursts triggered by isolated coal pillars and presented an energy distribution model under a static load for coal pillars. Chen [14] et al. studied the effect of temperature on rock burst hazards. Based on many accident cases, Xu et al. [15] studied the energy sources and main control factors of rock bursts. The formation mechanism of rock bursts is complicated.

Mature rock burst theories include the strength theory, the energy theory, the burst tendency theory, the three-criterion theory, and the instability theory. In recent years, scholars have made great achievements in researching the formation mechanism of rock bursts. Dai et al. [16], Hu et al. [17], and DOU et al. [18] studied the effect of faults on rock bursts. They believed that roof migration can activate faults and trigger rock bursts. Jiang [19, 20] studied the creep characteristics of deep coal masses under high stresses. Xu et al. [21] discussed the formation mechanism of rock bursts on the coalface based on microseismic monitoring results and obtained precursory information. Pan [22] et al. studied the formation mechanism of rock bursts when there are two soft coal seams. Yu et al. [23] studied the formation mechanism of rock bursts when there is an ultrathick conglomerate.

As previously mentioned, many studies have been conducted on the triggering factors and formation mechanism of rock bursts. However, few studies have considered the formation mechanism of rock bursts on the seam floor under an ultrathick roof conglomerate. Hence, further study is required. This paper is based on the rock burst accident that occurred on the fully mechanized coalface 13230 in the east-3 mining zone of coal seam 2-3 in the Gengcun Coal Mine, which includes the Yima Coal Field. Through a microseismic monitoring, a theoretical analysis, and a field investigation, this paper analyses the formation mechanism of floor rock bursts when an ultrathick conglomerate is mined, identifies the formation mechanism of rock bursts in the Yima Coal Field, and proposes specific control measures for the prevention and control of rock bursts in similar conditions.

2. Engineering Background

2.1. Overview of the Accident. At 10 : 42 : 20 on December 22, 2015, a rock burst occurred in the conveyor gateway on coalface 13230 in the Gengcun Coal Mine. According to the microseismic monitoring results, the seismic source was 830.7 m in front of the coalface and 3.0 m under the seam floor, which was 7.9 m away from the upper side of the conveyor gateway. The magnitude of the rock burst was 2.1, and the energy produced was 6.3×10^5 J. When the rock burst occurred, the roadway within 160 m from the end of the conveyor gateway to the coalface was immediately damaged: the floor bulged, both sides contracted, the hydraulic lifting device was seriously deformed, bent, and broken, and the equipment was overturned. The accident caused two deaths. The conditions at the accident site were as follows.

The cross section of the roadway was reduced to 3/4 of the original size, and the conveyor gateway, which was 80 m away from the most severely damaged coalface, was nearly closed. Among the 35 hydraulic lifting devices used for forepoling, 30 were damaged. The large stand columns were broken in seven of the lifting devices, bent in 11, and toppled over in 12; equipment trains were displaced or turned over; the belt was displaced or stopped running. The impact of the accident on the roadway of the conveyor gateway is shown in Figure 1:

2.2. Engineering Background of the Coalface Where the Accident Occurred. Coalface 13230 is in the east wing of the downhill roadway in the east-3 mining zone (2-3) of the Gengcun Coal Mine. In the north, the fully mechanized coalface 13210 has been mined. The west and south sides have unmined coal mass 2-3. The mine-out area of coalfaces 21121 and 21141 of the Qianqiu Mine lies to the east of the open-off cut, and the F_{16} faultage, with a drop height of 50–500 m, is 600–700 m underneath the cut. The coal seam 2–3 on this coalface has a thickness of 10.4 m, and the average mining depth is 633 m. The seam includes greyish-white sandy mudstone with a thickness of 280 m and a conglomerate bed with a thickness of 380 m over the roof of the coalface. With incomplete roof caving, the mine has a surface subsidence coefficient of 0.30–0.70. Below the conveyor gateway floor of the coalface, there is a 1.5-m-thick coal seam, and the seam floor contains low-strength carbonaceous mudstone with a thickness of 1–3 m. The roof and coal seam of the coalface have a high rock burst risk, while the floor features a low risk. Until the accident occurred, the coalface had advanced 32.8 m on average. For the relative position of the coalface, see Figure 2.

2.3. Formation Conditions of Rock Burst

2.3.1. Geostress Characteristics. Rock bursts are closely related to the geostress in a coal mass [24]. To ensure a thorough understanding of the geomechanical environment of the deep surrounding rocks in the Gengcun Coal Mine, we conducted geostress tests on the conveyor gateway of coalface 13230, the downhill roadway in the east-3 mining zone of the Gengcun Coal Mine, and the track gateway of coalface 21141 in the nearby Qianqiu Coal Mine (test point 1 was 250 m away from the conveyor gateway of coalface 13230; test point 2 was 380 m away from the conveyor gateway of coalface 13230; test point 3 was on the downhill roadway of coalface 13230; test point 4 was 55 m away from the track gateway of coalface 21141 in the Qianqiu Coal Mine). The layout of in-situ stress measuring points is marked in Figure 2(a). The test results are shown in Table 1.

According to the geostress test results, the stress of the primary rock is slightly higher than the medium level, and the four test points are all far away from the mined-out zone, which can reflect the stress of the primary rock. The three (75%) test points are dominated by vertical stress, and one (25%) test point has tectonic stress. Therefore, coalface 13230 and the area near the coal pillar between the mines are subject to both vertical stress and horizontal tectonic stress, creating stress conditions for the occurrence of rock bursts.

2.3.2. Ultrathick Conglomerate. The results show that the bending property of the roof is proportional to the fifth power of the roof overhang length. The more elastic energy is stored, the more likely the occurrence of a rock burst is [25]. After a large area of coalfaces 21101, 21221, and 21141 in the Qianqiu Coal Mine, which are located to the east of coalface 13230, was mined out, the mine has a surface subsidence coefficient of 0.30–0.70, with incomplete roof caving. A large

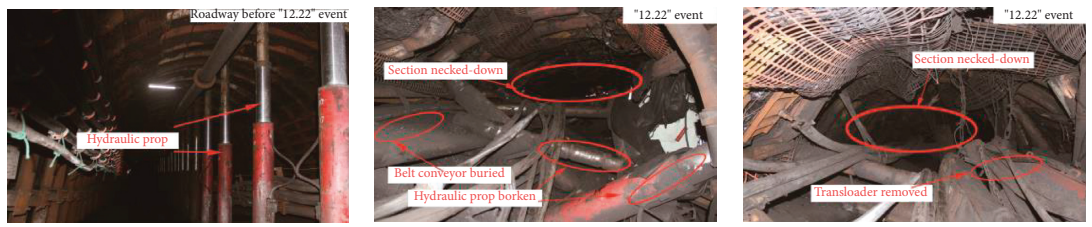

(a) (b) (c)

Figure 1: Photos of roadway's damage after the "12.22"event in the 13230 working face. (a) Transport gateway before "12.22″event. (b) Transport gateway when "12.22″event.

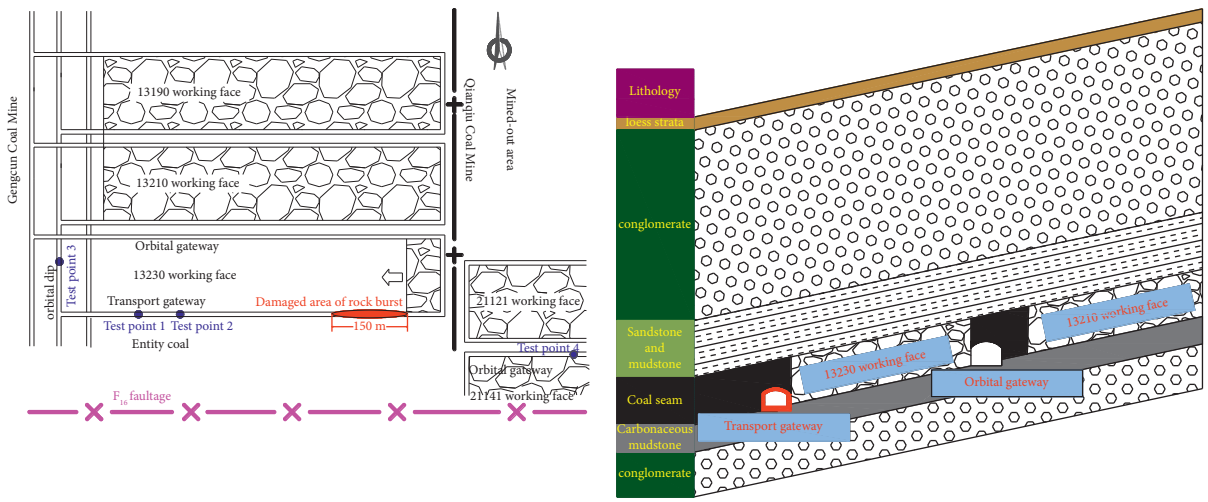

(a) (b)

Figure 2: Relative position of coalface 13230. (a) Planar view. (b) Profile.

Table 1: Geostress test results in the deep part of the Gengcun Coal Mine.

Test point	H (m)	σ_v (mpa)	σ_H (mpa)	σ_h (mpa)	k
1	621	15.53	12.58	7.09	0.81
2	622	15.55	13.93	7.29	0.89
3	599	14.98	14.84	7.69	0.99
4	633	15.83	17.51	9.05	1.11

H: buried depth of the test point, σ_v: vertical stress, σ_H: maximum horizontal stress, σ_h: minimum horizontal stress, and k: side pressure ratio.

area of the overlying ultrathick conglomerate is suspended, and the ultrathick conglomerate acts as a whole on the overlying strata below so that the stress is transferred to coalface 13230. As a result, the stress is concentrated in the advancing abutment of the coal seam, and coalface 13230 is under a relatively high vertical stress at the beginning of mining. High stress levels can easily produce very large pressures on coalfaces and even trigger rock bursts [26, 27].

2.3.3. F_{16} Thrust Faultage. The F_{16} faultage, with a drop height of 50–500 m, is located 600–700 m below coalface 13230. Based on the core exposed by geological drilling in the Gengcun Coal Mine, the extrusion force of the F_{16} faultage near the coalface causes the stratum cut by a normal fault to have a large-scale northward thrust-slip movement along the top face of the mudstone stratum. At the same time, the fault interface between blocks shows the characteristics of torsional faults due to the differential movement of fault blocks. The thrust caused by a large extrusion force of the fault and the instability of the overlying ultrathick conglomerate roof under the influence of dynamic pressure will also make the F_{16} faultage active [22]. The coal mass on coalface 13230 is under a high level of stress. Based on experience in adjacent mines, the position closer to the F_{16} faultage is more susceptible to rock bursts.

2.3.4. "Strong-Weak" Coal and Rock Structure. The area damaged by rock bursts of coalface 13230 leaves a coal floor with a thickness of 1.5–5 m and low-strength carbonaceous

mudstone with a thickness of 1–3 m on the floor. The part below the damaged area is directly connected with the basal conglomerate with a thickness of several metres to more than 10 m. Conglomerate and sandstone are hard, while coal seams and mudstone are soft. Clamped by the hard roof and floor, on the one hand, the coal seam suddenly ruptures at the side direction or gradually expands towards the mining space under high pressure. On the other hand, the resistance and deformation at the junction between the coal and the rock block the development of the previously mentioned process. In this case, there is a very high shear stress and a very high normal stress at the junction between the coal seam and the surrounding rock, which will trigger rock bursts once the stress exceeds a certain limit.

3. Mechanism of Floor Slip-Type Rock Burst

3.1. Estimation of Maximum Floor Bearing Capacity. After the underground roadway is excavated, the stress from the surrounding rock is redistributed, and a high abutment pressure zone appears in the leading section of the roadway. The soft floor has a low strength. Then, the roadway floor will have a slip field under the influence of abutment pressure [28, 29]. The plastic slip failure of the roadway floor is assumed to comply with the Mohr-Coulomb criterion. According to Prandtl's analysis of the ultimate bearing capacity in soil mechanics [24], an estimation model for the ultimate bearing capacity of floor slip is established, as shown in Figure 3. Assume that H is the burial depth of the roadway, m, c is the cohesive force, Mpa, and φ is the internal friction angle,°.

Depending on the stress field and movement trend, the floor slip field can be divided into an active zone COD, a transition zone BOC, and a passive zone AOB. The COD slip line field in the COD compresses in the vertical direction and expands in the horizontal direction under concentrated high stress levels. The entire large-area soft floor is squeezed to slip to the transition zone BOC in flow conditions. BOC is clamped by COD and AOB and transfers stress to AOB according to the motion trajectory under the compression and expansion of COD. As a result, the entire floor of AOB slips to the mining space, causing a rock burst on the seam floor.

According to the slip line field theory, there are two slip lines, that is, α cluster and β cluster. In COD and AOB, both α cluster and β cluster are straight, and the stress field is uniform. In BOC, α cluster is straight, while β cluster is logarithmic spiral, and BOC is a simple slip line field [30, 31].

In AOB, according to the related theory and analysis of Cauchy boundary values [32], the stress state of AOB S_{AOB} is as follows:

$$\begin{cases} S_{AOB} = \dfrac{c\ \cot\ \varphi}{1 - \sin\ \varphi}, \\ \theta = \pi. \end{cases} \tag{1}$$

θ is the angle between the first principal stress of AOB and the x-axis. It can be seen from formula (1) that the stress value at point B is $S_B = \mathrm{ccot}\varphi/1 - \sin\varphi$.

In BOC, according to the nature of the slip line field, the stress value of point B S_B and that of point C S_C on the same β cluster in BOC have the following relationship:

$$LnS_B + 2\theta_B \cot\ 2\ \mu = LnS_C + 2\theta_C \cot\ 2\mu, \tag{2}$$

where θ_B is the angle between the first principal stress at point B and the x-axis, $\theta_B = p$; θ_C is the angle between the first principal stress at point C and the x-axis; μ is the angle between α cluster and β cluster. We can obtain the stress value at point C S_C by substituting S_B at point B into formula (2):

$$S_C = \frac{c\ \cot\ \varphi \cdot e^{2\left(\pi - \theta_c\right)\cot 2\mu}}{1 - \sin\ \phi}. \tag{3}$$

In COD, the surface DO is the first principal stress plane, and the boundary conditions of the floor surface DO are as follows: the vertical stress is q_0, and the tangential stress is 0. Based on the theoretical analysis of mixed boundary values [33], the stress state of point C in COD can be obtained:

$$\begin{cases} S_C = \dfrac{q_0 + c\ \cot\ \varphi \cdot e^{\pi \tan \varphi}}{1 + \sin\ \phi}, \\ \theta = \dfrac{\pi}{2}. \end{cases} \tag{4}$$

According to the nature of the slip line field, we can obtain the stress value at point D S_D:

$$S_D = \frac{c\ \cot\ \varphi}{1 - \sin\ \phi} e^{\pi \tan \varphi}. \tag{5}$$

Based on formulas (4) and (5), the ultimate bearing capacity q_0 of the floor can be obtained as follows:

$$q_0 = c\ \cot\ \varphi \frac{1 + \sin\ \phi}{1 - \sin\ \phi} e^{\pi \tan \varphi} - c\ \cot\ \varphi. \tag{6}$$

According to the physical and mechanical properties of the coal seam 2-3, we can obtain the maximum bearing capacity of floor slip in the coal seam 2-3 using formula (6), that is, 26.3 MPa.

3.2. Estimation of Failure Depth of the Roadway Floor. According to the studies on how the mine pressure and rock stratum affect the failure scope of the mining floor, an estimation model for the failure scope of floor slip is established, as shown in Figure 4.

The slip line field theory and Rankine's earth pressure theory are used to analyse the maximum floor failure depth [34]: COD bears the active earth pressure P_a at active limit equilibrium; and DOA bears the passive earth pressure P_p at passive limit equilibrium.

$$P_a = \gamma\left(h_{\max} + h + h_g\right) - 2c\sqrt{K_a}, \tag{7}$$

$$P_p = \gamma h_{\max} K_p + 2c\sqrt{K_p}, \tag{8}$$

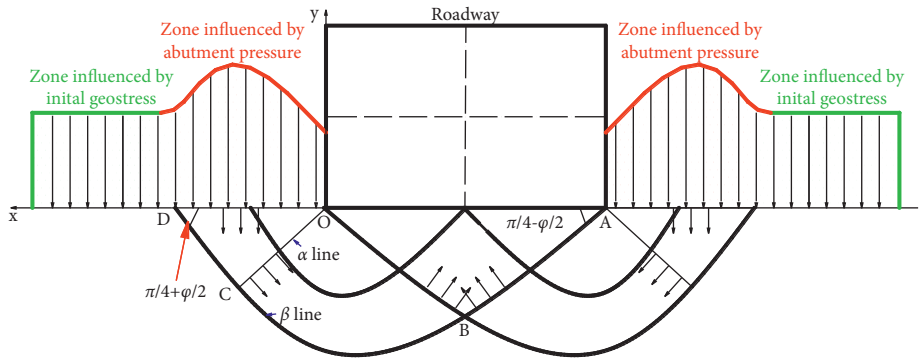

Figure 3: Estimation model for ultimate bearing capacity of floor slip.

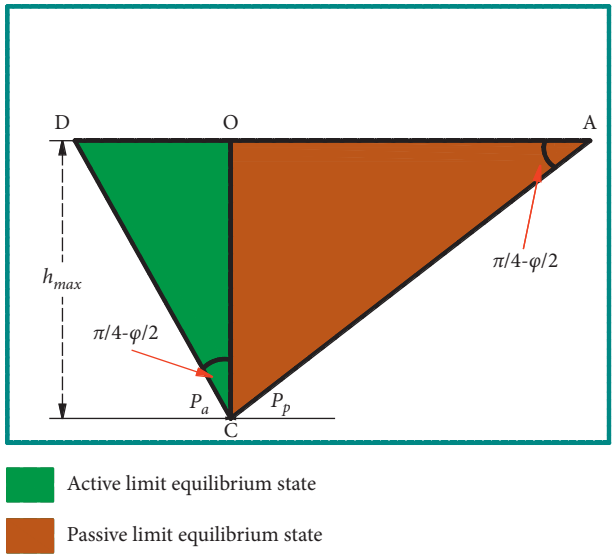

Figure 4: Estimation model for floor failure depth.

where the active earth pressure coefficient $K_a = \tan^2(45^\circ - \varphi)$ and the passive earth pressure coefficient $K_p = \tan^2(45^\circ + \varphi)$. Because point C is at limit equilibrium and the active earth pressure is equal to the passive earth pressure, the maximum failure depth of the roadway floor can be obtained as follows:

$$h_{\max} = \frac{(h_g + h)\tan^2(45^\circ - \phi/2) - 2c/\gamma}{\left[\tan^2(45^\circ + \phi/2) - \tan^2(45^\circ - \phi/2)\right]}. \quad (9)$$

$h_{\max}$ is the maximum failure depth of the roadway floor, m; γ is the average unit weight of the coal and rock over the floor, KN/m^3; h is the roadway height, m; and h_g is the height of the roadway pressure arch, m.

The height of the roadway on the coalface where the accident occurred is 4.2 m, and the internal friction angle of the coal and rock on the seam floor is 25°. The unit weight of the coal and rock over the floor is 2610 KN/m^3. From formula (9), we can estimate that the maximum failure depth of the floor on the coalface where the accident occurred is 5.39 m. The total thickness of the soft floor and bottom coal in the burst-stricken area is 7.93 m on average, which is close to the theoretically estimated maximum floor failure depth.

3.3. Estimation of Advancing Abutment Pressure. The mined-out zones of coalfaces 21121 and 21141 in the Qianqiu Coal Mine, with surface subsidence coefficients ranging from 0.30 to 0.70, are located to the east of coalface 13230. With incomplete caving, the roof is half overhang. The fracture height of the rock stratum is approximately half of the width of the mined-out zone. According to the analysis of the stress transmission mechanism of the half-suspended roof structure, the weight Q transferred to the coal mass on the adjacent coalface is 1/4 of the weight of the fault zone and 1/2 of the weight of the zone without fault on the overlying strata in the mined-out zone of the half-suspended roof. The angle o between the line connecting the separation end on one side of the mined-out zone and the horizontal direction is called the movement angle of the rock strata [20]. The estimation model for stress increment transferred from the high conglomerate stratum to the coal mass on one side of the coalface is shown in Figure 5.

The vertical stress $б_Q$ applied on the floor is composed of the abutment pressure $б_q$ generated by the dead weight of the overlying strata and the abutment pressure increment $\Delta б$:

$$\sigma_Q = \sigma_q + \Delta\sigma = \sigma_q + \sum_{i=1}^{n} \sigma_i. \quad (10)$$

Floor burst is likely to occur when the vertical principal stress applied on the floor exceeds the load carried by the floor. In formula (10), $б_q$ is the abutment pressure generated by the dead weight of the coal seam, and $\triangle б$ is the pressure transmitted from the suspended and exposed part of the ith key stratum to the coal mass on one side, $i = 1 \sim n$.

According to the conditions of coalface 13230 and its adjacent mined-out zone, we can estimate the stress using formula (10). Affected by the mined-out zones of coalfaces 21121 and 21141 in the Qianqiu Coal Mine, the strike abutment pressure of coalface 13230 produces an influence within 197 m, the peak stress is 98 m away from the coalface, and the maximum abutment pressure is 47.2 MPa. The maximum abutment pressure exceeds the bearing capacity of the seam floor, and the peak stress area appears close to the location where the most severe burst occurred (80 m away from the coalface).

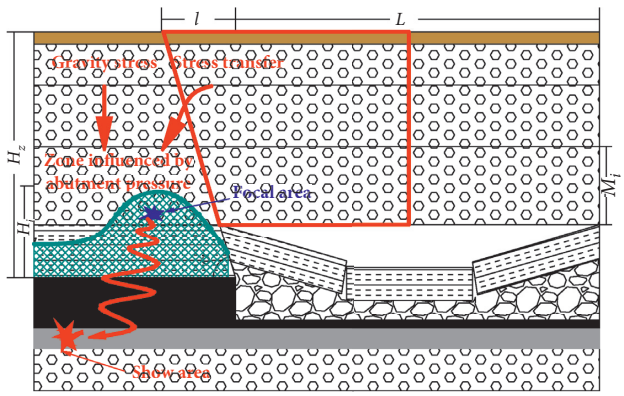

Figure 5: Estimation model for strike abutment pressure.

3.4. Formation Mechanism of Floor Slip Burst. After the coal seam is excavated, the coal mass in front of the coalface generates a high vertical stress under the influence of stress transfer because of the incomplete caving of the ultrathick conglomerate, and the coal seam expands under a high stress and results in plastic deformation [35–37]. Affected by the coupling of ultrathick conglomerate activity, excavation disturbance, and fault activation, burst will occur on the coalface when the load bearing limit of the coal mass is exceeded. In the meantime, the floor of the coalface undergoes plastic expansion under a high stress and creates a slip field at the bottom corner of the roadway. The burst failure and instability of the coal mass on the coalface enable the floor of the coalface to move along the slip line. When the bearing capacity of coal and rock mass is exceeded, a large-scale slip burst will be triggered instantly. Therefore, the floor slip burst occurs concurrently with the coal seam instability-caused burst. From the overturning direction of the equipment trains and pillars on the coalface where the accident occurred and the burst of coal mass in the roadway of the conveyor gateway, we can know that the expansion impact force comes from the two bottom corners of the roadway where the slip line field is roughly located.

4. Control of Rock Bursts

4.1. Control Method of Rock Bursts. According to the formation mechanism of rock bursts caused by overall floor slip and instability, we know that this type of rock burst is mainly related to the stress concentration and ultimate bearing capacity of the floor. Therefore, for the rock burst caused by floor slip and instability, we can stop the transfer of the floor stress to avoid the production of a slip line field, increase the floor bearing capacity, and reduce the concentration of coal stress on the coalface so that the high-stress zone will migrate to the deep coal mass.

(1) *Floor Pressure Relief.* Floor pressure relief holes can be drilled at the two bottom corners of the roadway, which are vertical to the side of the roadway, with a downward inclination angle of $45^\circ \pm 5^\circ$. The drill hole has a diameter of ≥120 mm and a hole pitch of 1 m, until the final hole reaches the hard rock stratum of the floor. Except for the floor pressure relief holes at the bottom corners of the roadway, 3-4 floor pressure relief holes can be drilled along the cross section of the roadway to prevent stress transmission along the roadway floor. The floor pressure relief holes can be drilled for charging and blasting. If the small depth of the floor pressure relief holes is not favourable for sealing and blasting, water can be injected into the floor pressure relief holes for softening.

(2) *Coal Pressure Relief.* Dense large-diameter pressure relief holes can be drilled on the coal mass at the side of the roadway to reduce the coal strength and expansion stress so that the abutment pressure can migrate to the deep part, creating conditions for the slow release of elastic energy. According to the estimated range of the advancing abutment pressure, coal pressure relief should be performed within 197 m in front of the coalface so that it can be extracted under low stress.

(3) *Reinforced Supports.* Within the key dangerous burst area and the influence range of the advancing abutment pressure on the coalface, in addition to the original anchor rod, anchor cable, anchor net, and 36U-shaped shed, a gate-type antiburst support and a hydraulic lifting device can be used to reinforce the supports to further improve the compression resistance, burst resistance, protection capability, and floor bearing capacity of the roadway. The basic and reinforced supports of the roadway on-site are shown in Figure 6.

4.2. Control Effect of Rock Bursts. Microseismic monitoring technology is based on seismology and acoustic emission. The rock burst prevention and control effect can be indirectly assessed by arranging sensors to monitor and collect microseismic signals when a microseismic energy event occurs. An ESG (Engineering Seismology Group, Kingston, Canada) microseismic monitoring system was installed on coalface 13230, with one ESG microseismic sensor deployed every 200 m in the track gateway and conveyor gateway, which covers the entire mining area of coalface 13230. The microseismic monitoring arrangement is shown in Figure 7.

The microseismic energy evolution characteristics can be obtained by analysing the microseismic energy prior to the rock burst on coalface 13230. As shown in Figure 8, before the rock burst accident occurred, only a few low-energy microseismic events occurred, and there were no obvious signs prior to these events. After the rock burst occurred, the mine was shut down. Without excavation disturbance on the coalface, the overlying ultrathick conglomerate was relatively stable. There are a few microseismic events that are all less than the "fourth power," resulting in low energy. After production was resumed at the coalface, by taking measures including floor breaking, dense drilling of the coal mass for pressure relief, and gate-type supporting, microseismic energy events of the "fifth power" accounted for 5%, those of the "fourth power" accounted for 60%, and those of the "third power" accounted for 30%. At the end of mining on the coalface, despite the dynamic phenomenon, no

Figure 6: Basic and reinforced supports of the roadway.

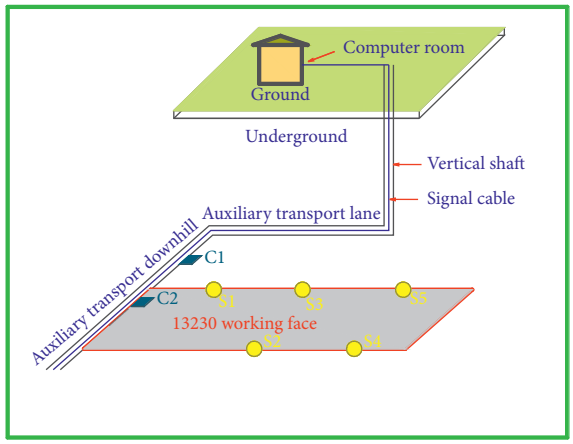

Figure 7: ESG microseismic monitoring arrangement.

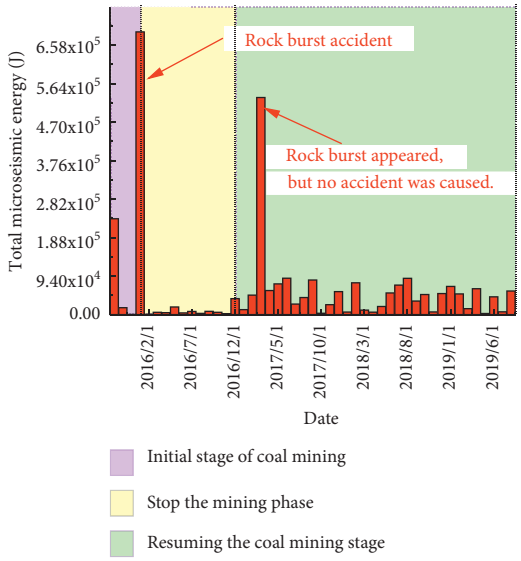

Figure 8: Microseismic energy evolution before and after production resumption.

destructive rock burst accident occurred under the reinforced protection of the gate-type support. The mining on this face was smoothly completed in June 2020.

5. Conclusion

(1) The formation mechanism of the rock burst on coalface 13230 in the Gengcun Coal Mine is obtained. Due to the insufficient collapse of the giant thick conglomerate overlying the working face, the leading abutment pressure of the working face is greater than the bearing capacity of the floor, and then the rock burst occurs.

(2) An estimation model for the ultimate bearing capacity and failure depth of floor slip is established. The ultimate bearing capacity of the floor is 26.3 MPa. When the ultimate bearing capacity is exceeded, the roadway floor of the coalface may undergo overall slip burst. The maximum floor failure depth is 5.39 m, which exceeds the total thickness of part of the roadway bottom coal and direct floor.

(3) An estimation model for advancing abutment pressure in the case of insufficient roof caving is established. The advancing abutment pressure produces an influence within 197 m ahead of the coalface. The peak value zone is within 98 m in front of the coalface. The peak stress is 47.2 MPa. These estimated results basically coincide with the failure scope and strength of the rock burst.

Data Availability

The data used to support the findings of this study are available from the corresponding author upon request.

Conflicts of Interest

The authors declare that they have no conflicts of interest.

Acknowledgments

This study was supported by the National Natural Science Foundation of China (grant nos. 41977252 and U2005205); the State Key Laboratory of Geohazard Prevention and Geoenvironment Protection Independent Research Project (grant no. SKLGP2020Z001); and the State Key Laboratory of Geohazard Prevention and Geoenvironment Protection

Open Fund (grant nos. SKLGP2019K010 and SKLGP2020K015).

References

[1] M. T. Gao, Z. Q. Song, and H. Q. Duan, "Mechanical properties and control rockburst mechanism of coal and rock mass with bursting liability in deep mining," *Shock and Vibration*, vol. 2020, Article ID 8833863, 15 pages, 2020.

[2] Q. Zhang, E. Wang, X. Feng, C. Wang, L. Qiu, and H. Wang, "Assessment of rockburst risk in deep mining: an improved comprehensive index method," *Natural Resources Research*, vol. 30, no. 2, pp. 1817–1834, 2021.

[3] C. Zhu, K. Zhang, H. Cai et al., "Combined application of optical fibers and CRLD bolts to monitor deformation of a pit-in-pit foundation," *Advances in Civil Engineering*, vol. 2019, no. 1, 16 pages, Article ID 2572034, 2019.

[4] C. Zhu, M. C. He, Z. G. Tao, Q. X. Meng, and X. H. Zhang, "Recognition and prevention of rockfall vulnerable area in open-pit mines based on slope stability analysis," *Geomechanics and Engineering*, vol. 26, no. 5, pp. 441–452, 2021.

[5] X. Li, K. Peng, J. Peng, and D. Hou, "Experimental investigation of cyclic wetting-drying effect on mechanical behavior of a medium-grained sandstone," *Engineering Geology*, vol. 293, p. 106335, 2021.

[6] X. Li, K. Peng, J. Peng, and H. Xu, "Effect of cyclic wetting-drying treatment on strength and failure behavior of two quartz-rich sandstones under direct shear," *Rock Mechanics and Rock Engineering*, vol. 54, no. 11, pp. 5953–5960, 2021.

[7] M. Z. Gao, J. Xie, Y. N. Gao et al., "Mechanical behavior of coal under different mining rates: a case study from laboratory experiments to field testing," *International Journal of Mining Science and Technology*, vol. 31, pp. 825–841, 2021.

[8] M. Gao, J. Xie, J. Guo, Y. Lu, Z. He, and C. Li, "Fractal evolution and connectivity characteristics of mining-induced crack networks in coal masses at different depths," *Geomechanics and Geophysics for Geo-Energy and Geo-Resources*, vol. 7, no. 1, p. 9, 2021.

[9] L. Guo, C. J. Zhou, and Z. Ru, "Underground engineering rock burst review of Research," *Applied Mechanics and Materials*, vol. 2156, pp. 1161–1166, 2013.

[10] B. Jiang, H. Ji, L. Fu, S. Gu, T. Zou, and J. Lu, "Research on evaluation index and application of rockburst risk in deep strip mining," *Shock and Vibration*, vol. 2020, no. 1, 10 pages, Article ID 8824323, 2020.

[11] W. Cai, X. Bai, G. Si, W. Cao, S. Gong, and L. Dou, "A monitoring investigation into rock burst mechanism based on the coupled theory of static and dynamic stresses," *Rock Mechanics and Rock Engineering*, vol. 53, no. 12, pp. 5451–5471, 2020.

[12] B. Wang, S. Zhu, F. Jiang, J. Liu, X. Shang, and X. Zhang, "Investigating the width of isolated coal pillars in deep hard-strata mines for prevention of mine seismicity and rockburst," *Energies*, vol. 13, no. 17, p. 4293, 2020.

[13] D. Li, J. Zhang, Y. Sun, and G. Li, "Evaluation of rockburst hazard in deep coalmines with large protective island coal pillars," *Natural Resources Research*, vol. 30, no. 2, pp. 1835–1847, 2021.

[14] G. Chen, T. Li, G. Zhang, H. Yin, and H. Zhang, "Temperature effect of rock burst for hard rock in deep-buried tunnel," *Natural Hazards*, vol. 72, no. 2, pp. 915–926, 2014.

[15] L. M. Xu, K. X. Lu, Y. S. Pan, and Z. J. Qin, "Study on rock burst characteristics of coal mine roadway in China," *Energy Sources, Part A: Recovery, Utilization, and Environmental Effects*, vol. 2019, Article ID 1655114, 2019.

[16] L. P. Dai, Y. S. Pan, and Z. H. Li, "Quantitative mechanism of roadway rockbursts in deep extra-thick coal seams: theory and case histories," *Tunnelling and Underground Space Technology*, vol. 111, Article ID 103861, 2021.

[17] S. C. Hu, Y. L. Tan, and J. G. Ning, "Multiparameter monitoring and prevention of fault-slip rock burst," *Shock and Vibration*, vol. 2017, Article ID 7580109, 8 pages, 2017.

[18] G. A. Zhu, L. M. Dou, and Y. Liu, "Dynamic behavior of fault slip induced by stress waves," *Shock and Vibration*, vol. 2016, Article ID 4386836, 13 pages, 2016.

[19] M. Zhang and F. Jiang, "Rock burst criteria and control based on an abutment-stress-transfer model in deep coal roadways," *Energy Science & Engineering*, vol. 8, no. 8, pp. 2966–2975, 2020.

[20] S. T. Zhu, D. C. Ge, and F. X. Jiang, "Rock burst mechanism under coupling action of working face square and regional tectonic stress," *Shock and Vibration*, vol. 2021, Article ID 5538179, 11 pages, 2021.

[21] C. Xu, Q. Fu, X. Cui, K. Wang, Y. Zhao, and Y. Cai, "Apparent-depth effects of the dynamic failure of thick hard rock strata on the underlying coal mass during underground mining," *Rock Mechanics and Rock Engineering*, vol. 52, no. 5, pp. 1565–1576, 2019.

[22] J. F. Pan, S. H. Liu, and S. W. Wang, "A new theoretical view of rockburst and its engineering application," *Advances in Civil Engineering*, vol. 2018, Article ID 4683457, 12 pages, 2018.

[23] Z. X. Yu, J. L. Wen, and H. T. Ma, "Research on the evolution law of spatial structure of overlying strata and evaluation of rock burst risks in deep well strip mining," *Geotechnical & Geological Engineering*, vol. 2021, pp. 1–13, 2021.

[24] W. J. Guo, Y. Y. Li, and D. W. Yin, "Mechanisms of rock burst in hard and thick upper strata and rock-burst controlling technology," *Arabian Journal of Geosciences*, vol. 9, no. 10, Article ID 2596, 2016.

[25] J. Wen, H. Li, F. Jiang, Z. Yu, H. Ma, and X. Yang, "Rock burst risk evaluation based on equivalent surrounding rock strength," *International Journal of Mining Science and Technology*, vol. 29, no. 4, pp. 571–576, 2019.

[26] W.-Y. Guo, T.-B. Zhao, Y.-L. Tan, F.-H. Yu, S.-C. Hu, and F.-Q. Yang, "Progressive mitigation method of rock bursts under complicated geological conditions," *International Journal of Rock Mechanics and Mining Sciences*, vol. 96, pp. 11–22, 2017.

[27] M. C. He, J. Y. Li, and F. Q. Ren, "Rock burst criterion based on clay mineral content," *Arabian Journal of Geosciences*, vol. 13, no. 4, pp. 1–8, 2020.

[28] Y. Zhao, N. Liu, X. Zheng, and N. Zhang, "Mechanical model for controlling floor heave in deep roadways with U-shaped steel closed support," *International Journal of Mining Science and Technology*, vol. 25, no. 5, pp. 713–720, 2015.

[29] Y. Yang, S. Wei, and S. Zhao, "Research on the destructional pattern of surrounding rock of roadway induced by dynamic disturbance," *Geotechnical & Geological Engineering*, vol. 37, no. 5, pp. 4447–4459, 2019.

[30] Z. J. Li, S. B. Li, and X. L. Zhao, "Floor heave controlling technology of deep soft rock roadway," *Applied Mechanics and Materials*, vol. 170–173, pp. 68–71, 2012.

[31] Y. Qiu, Y. H. Lu, C. A. You, and Q. Y. Liu, "Parameter design of anti-slide pile control method in floor heave," *Applied Mechanics and Materials*, vol. 170–173, pp. 541–544, 2012.

[32] P. Dang, J. Y. Du, and T. Qian, "Boundary value problems for periodic analytic functions," *Boundary Value Problems*, vol. 2015, no. 1, pp. 1–28, 2015.

[33] D. A. Giuseppina, "Multiplicity results for nonlinear mixed boundary value problem," *Boundary Value Problems*, vol. 2012, no. 1, pp. 1–12, 2012.

[34] M. Iskander, Z. Chen, M. Omidvar, and I. Guzman, "Rankine pseudo-static earth pressure for c-ϕ soils," *Mechanics Research Communications*, vol. 51, pp. 51–55, 2013.

[35] X. F. Shi, X. K. Zhang, and F. X. Jiang, "Study on practice of rockburst accident prevention in multi-seam mining controlled by large fault and hard roof," *Geotechnical & Geological Engineering*, vol. 38, pp. 1–11, 2020.

[36] F. Xiong, Q. Jiang, and C. Xu, "Fast equivalent micro-scale pipe network representation of rock fractures obtained by computed tomography for fluid flow simulations," *Rock Mechanics and Rock Engineering*, vol. 54, no. 2, pp. 937–953, 2021.

[37] F. Xiong, C. Zhu, and Q. Jiang, "A novel procedure for coupled simulation of thermal and fluid flow models for rough-walled rock fractures," *Energies*, vol. 14, p. 951, 2021.